SMAR 2019 – Fifth Conference on Smart Monitoring,
Assessment and Rehabilitation of Civil Structures

SMAR 2019

SMA-Reinforced Concrete Shear Walls Subjected to Reverse Cyclic Loading

Mena MORCOS [1], Dan PALERMO [1]

[1] Department of Civil Engineering, York University, Toronto, Canada

Contact e-mail: dan.palermo@lassonde.yorku.ca

ABSTRACT: The endeavour to develop earthquake-resilient structures has given popularity to an emerging material, Shape Memory Alloys (SMAs), by researchers over the last decade as an alternative novel solution to conventional steel reinforcement. SMAs recover induced strains in two unique ways, through unloading as a Superelastic (SE) material, or by the application of heat in the Shape Memory form. A SE-SMA-reinforced concrete component is expected to exhibit a self-centering phenomenon. Shear walls are routinely selected as the seismic force resisting system in concrete construction in Canada. For this reason, shear walls are considered for the inclusion of SE-SMAs as principal reinforcement in critical areas. The focus of this paper is to present experimental results of a slender concrete shear wall reinforced with SE-SMA reinforcement. Testing illustrated the capacity of the wall to recover inelastic displacements to a larger extent in comparison to a companion conventional steel-reinforced wall.

1 INTRODUCTION

The application of Shape Memory Alloys (SMAs) in structural engineering has given realization to smart structures that are resilient to seismic activity. Traditionally, Reinforced Concrete (RC) structures are designed to experience reinforcement yielding and concrete damage as a means to dissipate the seismic energy, which leads to permanent lateral deformations. A structure sustaining a residual drift of approximately 2.5% is deemed structurally unfit to serve its purpose and therefore requires complete replacement (Yazgan 2010). By integrating SMAs into RC structures as alternative reinforcement, structures experience significantly reduced residual drifts due to self-centering, where the seismic energy is dissipated in a manner which minimizes damage and economizes the cost of post-disaster repair (Menna et al. 2015).

Shape Memory Alloys are available through a variety of base metals such as copper (Cu) and iron (Fe). Cladera et al. (2014) and Shahverdi et al. (2016) demonstrated the applications of iron-based SMA reinforcement, however, Nitinol (NiTi) is a common researched SMA for structural applications as an alternative to conventional black carbon steel reinforcement (Alam 2007). Nitinol SMA is an alloy composed of approximately 56% Nickel and 44% Titanium (Abdulridha et al. 2013). Nitinol exhibits either the superelastic or shape memory phenomena dependent on the annealing process to achieve either the Austenite or Twinned Martensite material phase, respectively. In the superelastic state, Nitinol can recover from up to 6-8% axial straining upon unloading. In the shape memory state, Nitinol retains its deformed shape and recovers through the application of heat.

Superelastic Nitinol is appealing for structural applications due to its capacity to recover from large deformations, energy dissipation capacity, and high resistance to fatigue and corrosion (Ozbulut et al. 2011).

Various research efforts have demonstrated the wide structural applications of Nitinol. Recent studies relevant to shear walls include the work of Saiidi and Wang (2006) where SE-Nitinol was implemented as principle reinforcement in a bridge pier column. In addition, Abdulridha and Palermo (2017) investigated hybrid SMA-steel-reinforced slender shear walls. Another study that has shed light on the response of superelastic SMA was conducted by Youssef et al. (2008) on SMA-reinforced beam-column joints. Nitinol has also been used externally to retrofit shear walls (Cortés-Puentes and Palermo 2017).

This paper presents experimental results to highlight the self-centering capacity of a SE-SMA-reinforced concrete slender shear wall subjected to quasi-static lateral reverse cyclic loading.

2 CONSTRUCTION OF SHEAR WALL SPECIMENS

The shear walls in this study are detailed according to the seismic provisions of CSA A23.3 (2004). The dimensions followed a study previously completed by Abdulridha (2013). Each wall maintains an aspect ratio of 2.2, with a height of 2200mm, a length of 1000mm, and a thickness of 150mm. Each wall was built on a 500mm deep, 1600mm long and 1000mm wide foundation block. The top of each wall has a 400mm by 400mm cap beam, with a length of 1600mm.

Two shear walls were constructed: a steel-reinforced wall (SWS-R), and a SMA-reinforced wall (SWN). The ‘S-R’ following the initials for shear wall (SW) denotes steel-reinforced (S) with local repairs (-R). The base of SWS-R was locally repaired with Self-Consolidating Concrete (SCC) to replace regions of poorly consolidated concrete. The ‘N’ following ‘SW’ denotes Nitinol-reinforced. The reinforcement cages for each wall were generally assembled with 10M bars (100mm^2 and 11.3mm nominal diameter) in the principle and transverse directions, as well as for buckling-prevention ties. Principle reinforcement was distributed within two curtains, each curtain containing two bars in the boundaries and three bars across the web. The shear reinforcement was spaced at 150mm over the height of the wall. The buckling prevention ties were spaced at 75mm up to a height of 1100mm and spaced at 150mm thereafter. Wall SWN followed the same reinforcement details as the control wall (SWS-R), however, the steel bars within the boundaries were replaced by SE-Nitinol SMA bars. The Nitinol SMA reinforcement were smooth with a 12.7mm-diameter. The length of the SMA bars was limited to the height of the plastic hinge region. The ends of the SMA bars and adjoining steel bars were mechanically headed to allow for coupling, which occurred at a depth of 300mm below the top of the foundation block and at 900mm above the foundation within the boundary elements of the wall.

Wall SWS-R was cast with 30MPa concrete (14mm coarse aggregate), which reached 50.8MPa on the day of testing. The repair region of SWS-R was cast with Sika Sikacrete-08 SCC (8mm aggregate), reaching 73.4MPa on the day of testing. Wall SWN was cast with 30MPa concrete (14mm coarse aggregate), which reached 39.3MPa on the day of testing.

3 EXPERIMENTAL PROGRAM

The test setup was assembled using a set of four 6m-high structural steel columns, and four beams with the same section size. The four columns were positioned at each corner of the walls. The columns were anchored to the strong floor and connected at the height of the cap beam of the walls with the beams to stiffen the test frame. The two beams fastened parallel to the length of the walls supported the lateral bracing system. Each of these two beams supported an adjustable set of rollers meant to provide resistance against out-of-plane motion during testing. The rollers were adjusted until contact was made along the cap beam to an extent that did not induce resistance against in-plane translation.

The lateral displacements were imposed on the cap beam through a hydraulic actuator. The loading protocol included a sequence of target displacements based on recommendations of FEMA 461 (2007) and the guidelines of the ATC-24 (1992). Preliminary pushover analyses were performed for each wall to estimate the yield displacements. A terminal drift of 5% was selected to ensure severe strength deterioration as recommended by ATC-24 (1992). The target displacements were modified as a single loading history suitable for both walls. The target displacements initiated at 0.05% (1.2mm) drift, followed by 0.1% (2.4mm) drift, and then incrementally increasing by 0.1% up to 0.5% (12mm); these represent smaller seismic excursions. Thereafter the target displacements incrementally increased by 0.5% up to 5.0% (120mm), representing larger seismic demands. Each displacement level was cycled three times up to and including 1.0% drift, and two cycles per displacement thereafter for Wall SWS-R. Wall SWN experienced three cycles for each displacement up to and including 2.0% drift, and two cycles per subsequent displacement levels.

Monitoring the behaviour of the walls involved 32 strain gauges on the reinforcement cage, and 18 external sensors. A combination of cable and linear potentiometers were used to measure external displacements. The strain gauges and potentiometers were mounted to the same locations on each wall. The instruments were positioned to measure: displacements relative to the test frame and the lab strong floor, displacements along the height of the wall, sliding at the base of the wall, sliding of the foundation, vertical displacements at the cap beam and at 200mm above the base of the wall, shear strain, and uplift of the foundation. The monitoring of SWN differed in the use of post-yield strain gauges applied to the SMA reinforcement within the boundary elements and an additional four strain gauges applied to the outer SMA reinforcing bars embedded in the foundation block to measure yield penetration.

4 TEST RESULTS

The experimental drift-load response for each wall is presented in Figure 1. The performance points for each wall were determined by the method prescribed by Park (1989). The values presented in Table 1 are based on the average of the positive and negative loading directions. [Note: The ultimate displacement corresponds to the displacement level that sustains two repetitions of loading without experiencing a drop in lateral load capacity exceeding 20%.]

Wall SWS-R was tested first. The loading history was initiated with a lateral displacement of 1.2mm (0.05% drift). Visual inspection of the wall revealed hairline-flexural cracks at approximately 150mm above the base. At a displacement of 2.4mm (0.1% drift), a flexural crack had propagated across the entire wall at a height of 350mm from the base. The wall was then displaced to 4.8mm (0.2% drift) where shear cracking was observed at approximately 950mm from the base from both sides of the wall. In addition, flexural cracks fully propagated across the wall, spaced approximately 150mm over

the height of the plastic hinge. At 7.2mm (0.3% drift) and to 9.6mm (0.4% drift) the wall exhibited continued flexural damage within the plastic hinge region, and one horizontal crack across the wall at a height of 1250mm.

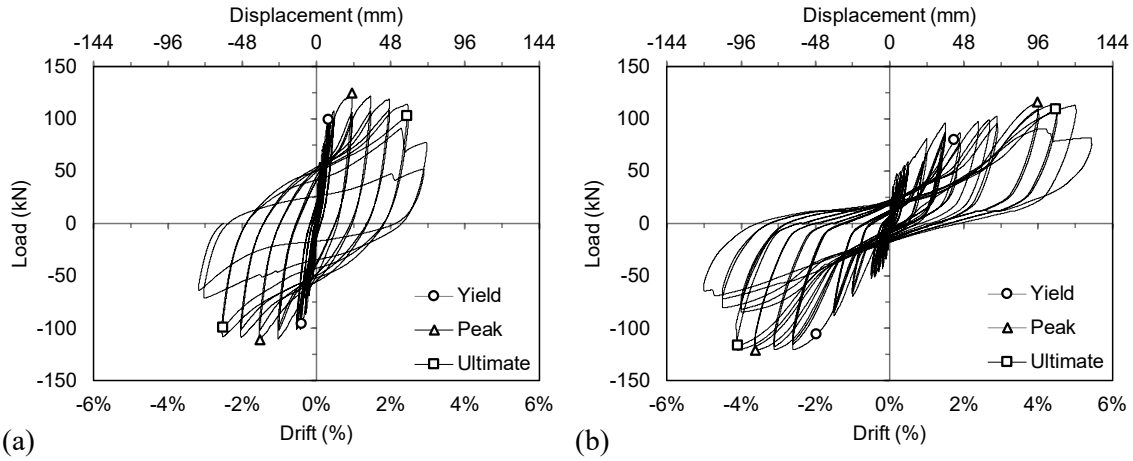

Figure 1. Lateral load-drift responses: (a) Wall SWS-R; and (b) Wall SWN.

Table 1. Performance points

Wall	Yield			Peak			Ultimate			μ
	δ (mm)	Drift (%)	Load (kN)	δ (mm)	Drift (%)	Load (kN)	δ (mm)	Drift (%)	Load (kN)	
SWS-R	8.7	0.36	97	30	1.25	118	60	2.5	101	6.9
SWN	45	1.88	93	91	3.80	118	103	4.29	113	2.3

Note: δ denotes lateral displacement; μ denotes ductility.

By the end of the 12mm displacement cycles (0.5% drift), a major crack along the base of the wall and the beginning of shear cracks from both sides at a height of 1400mm became evident. The 24mm displacement level (1.0% drift) induced the propagation of existing shear cracks and the development of new shear cracks following a fanning pattern from the upper half of the wall, as well as one dominant shear crack running across the plastic hinge. At a displacement of 36mm (1.5% drift) vertical cracking developed at the bottom of the wall near the edges of the boundary elements. By the end of 48mm of lateral displacement (2.0% drift), significant cracking was evident around the toe of the wall at each end. The onset of spalling was also observed surrounding the right toe. At the end of the displacement cycles to 60mm (2.5% drift), the right toe of the wall experienced widespread crushing. The left toe exhibited more spalling of large pieces of concrete as well as separation of the cover over the thickness of the wall up to approximately 150mm from the base. The crushing was predominately in the regions repaired with SCC.

The final imposed lateral displacement for SWS-R was 72mm (3.0% drift). During the first excursion of loading in the positive direction, two reinforcing bars fractured at approximately 40mm above the foundation near the outer face of the left boundary element. This resulted in a drop in the lateral load capacity. During the subsequent loading in the negative direction, a reduced reloading stiffness was

recorded in the load-displacement response, followed by rupturing of the two reinforcing bars near the outer face of the right boundary element at approximately 50mm above the foundation. The second excursion in the positive loading direction led to rupturing of the second row of reinforcing bars in the left boundary. Loading was terminated at the conclusion of the second excursion in the negative direction.

For wall SWN, a displacement of 1.2mm initiated a crack along the base penetrating approximately 400mm across the wall. At the completion of the displacement cycles to 2.4mm, the crack along the base propagated across the entire length of the wall. By the completion of loading to 4.8 mm of displacement, a flexural crack developed at approximately 300mm above the foundation reaching 900mm across the wall, in addition to the initiation of a flexural-shear crack at about 150mm above the base. Loading to 7.2mm of displacement induced a flexural-tension crack above the plastic hinge region at approximately 1100mm above the base. In addition, three vertical cracks positioned symmetrically about the centerline of the wall surfaced. The location of these cracks aligned with the longitudinal steel reinforcement in the web and were observed at an average height of 350mm from the base. A horizontal crack had also developed across the center of the wall, terminating at approximately 200mm from each end. Furthermore, a major horizontal crack developed across the length of the wall at about 300mm above the base. The displacement cycles to 9.6mm resulted in the propagation of the vertical cracks towards the top and base of the wall reaching an average length of 200mm. An additional horizontal crack developed from the center of the wall at a height of 650mm. The flexural crack that initiated at 1100mm above the base extended across the length of the wall. The major flexural-tension crack at 300mm widened to a greater extent in comparison to other cracks. The displacement to 12mm caused only minor propagations of the vertical cracks, by an average of 50mm, and the horizontal cracks located near the center of the wall lengthened by 150mm. At 24mm displacement, additional flexural cracks surfaced, the highest located at 1550mm from the base. At 36mm of lateral displacement numerous flexural-shear cracks surfaced fanning towards the plastic hinge region. At this point, the widths of the major horizontal cracks at 300mm and at the base were approximately 3mm. In comparison, all other crack widths were significantly smaller.

At 48 mm of lateral displacement, additional flexural-shear cracks became evident, the highest at 1900mm from the base. Existing cracks continued to propagate. At the peak of the loading, the major horizontal crack reached a width of 6mm, and the base crack widened to 14mm. Upon unloading, the crack widths were 0.5mm and 9mm, respectively. At 60mm displacement, spalling initiated about the major crack, approximately 170mm long and 20mm wide near the right edge of the wall.

At a displacement of 72mm it was very apparent that the wall was rocking about the major crack and the crack along the base. At the peak of the loading during the first cycle, crushing initiated at the right toe. The load-drift response plateaued through 84mm of displacement. At 96mm of displacement, the opening at the base was 38mm, while it was only 5mm at the major horizontal crack above the base. Additional concrete crushing was sustained by each toe, along with the development of new flexural-shear cracks near the top of the wall. Loading to the first excursion in the negative direction to 108mm of lateral displacement, resulted in rupture of the web vertical reinforcing bars near the right half of the wall. The web vertical reinforcing bars along the centerline ruptured during the first excursion of loading in the negative direction to 120mm displacement. In addition, local buckling of the web reinforcing bars to the left of the wall was observed. The second excursion of loading in the positive direction lead to rupturing of the web reinforcement to the left of the wall. Loading was terminated at the end of the 120mm displacement level. No apparent damage was visible to the SE-Nitinol bars in the boundaries.

5 DICSUSSION

The damage to SWN was dominated by two wide horizontal cracks that extended along the length of the wall, the larger one along the base, and the other at 300mm above the base. Wall SWS-R sustained widespread cracking and significant crushing at the toes and spalling along the base. The average crack width in SWS-R was 3mm (largest 8mm, smallest 1.25mm), recovering by an average of 36%. The average crack width throughout SWN was 0.08mm (largest 0.15mm, smallest hairline <0.10mm), with an average recovery of 82% upon unloading. The average width of the two largest cracks was 8.5mm, which on average recovered by 40%. Figure 2 demonstrates the extent of damage sustained by each wall at 2.5% drift.

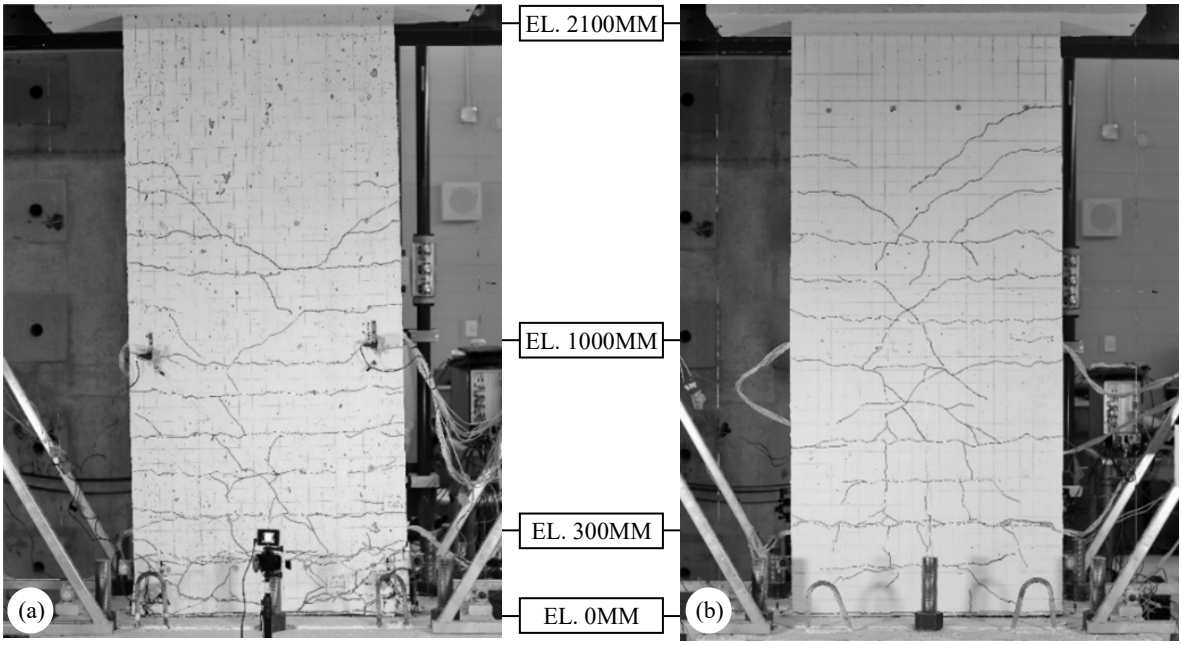

Figure 2. Damage due to 2.5% drift: (a) SWS-R; and (b) SWN.

Wall SWN demonstrated significant recovery due to the self-centering capacity inherent from the SE-SMA reinforcement. Displaced to 2.5% lateral drift, the average recovery was 55%; 66% from the positive loading direction, and 45% from the negative loading direction. [Note that the recovery from negative loading is relative to 4% drift due an error during loading]. In contrast, SWS-R recovered approximately 26% of the lateral displacements for each of the positive and negative loading directions. A comparison of the first cycle to 2.5% drift for each wall is presented in Figure 3.a.

The displacement ductility value of Wall SWS-R suggests a lateral capacity that is three times greater than Wall SWN, however, SWN attained an ultimate displacement of 103mm, compared to 60mm for SWS-R. Tazarv and Saiidi (2017) highlighted that drift is a more suitable measure to assess lateral performance. For this study, the drift for each wall, over a height of 2400mm, is 2.5% (SWS-R) and 4.3% (SWN).

SWS-R experienced significantly more base translation (sliding) than SWN. Sliding at the base of SWS-R was partially limited to a range of -4mm to 4mm only to the end of the first cycle to 1.5%

drift. Hereafter the range of sliding increased by an average of 3mm and continued to skew in the positive direction. Through the second excursion to 1.5% drift, the range of sliding was -2mm to 8mm, coinciding with the onset of cracking surrounding the toes of the wall. Through the displacement cycles to 2% drift, the range of sliding shifted, becoming 1mm to 12mm for the first cycle and then 8mm to 19mm for the second cycle, as cracking significantly increased at each toe. The initial displacement to 2.5% drift completely crushed the right toe causing sliding to 28mm. The monitoring sensor was then removed for protection before the completion of loading in the negative direction for the first cycle. The positive-skew and increase in the range of sliding in SWS-R can be attributed to the crushing of both toes and spalling along the base which reduced contact area upon loading in both directions. Furthermore, rupturing of the longitudinal bars in the boundary zones reduced the resistance to sliding. Sliding at the base of SWN was limited to a range of -14mm to 9mm throughout testing to 5% drift. The magnitude of sliding in SWN can be attributed to the onset of minor crushing at the toes from displacement to 4%, and the gradual rupturing of all six longitudinal bars in the web through displacements to 5% drift. A comparison of the magnitude of sliding for each wall is presented in Figure 3.b. The shape of the sliding response for SWN is similar to the load-drift response, signifying the self-centering capacity of the wall.

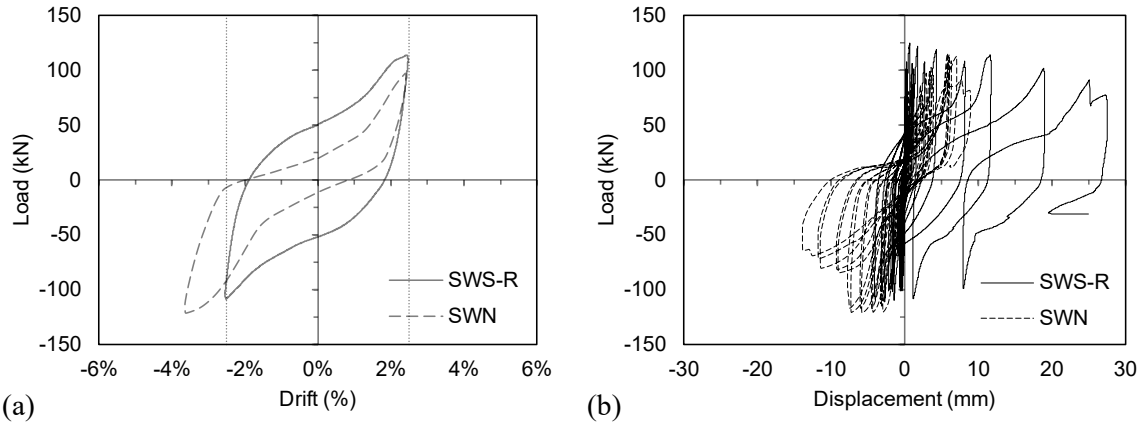

Figure 3. (a) 1st cycle at 2.5% drift; and (b) sliding at base of wall.

6 CONCLUSIONS

This experimental study focused on the self-centering capacity of a SE-SMA-reinforced slender shear wall (SWN) in comparison to a control wall (SWS-R). The walls were tested to a sequence of gradually increasing drifts through reverse cyclic loading. The following conclusions are drawn from the experimental results:

1. The SMA-reinforced wall recovered 66% of the lateral displacements from a benchmark drift of 2.5% (less than 1% residual drift), in comparison to a drift recovery of 26% for the control specimen.
2. Most cracks in the SMA-reinforced wall recovered by approximately 82%, and 40% for the major horizontal cracks, upon unloading from an imposed drift of 2.5%. The average width of the cracks was 0.08mm, in comparison to about 3mm in the control wall.

3. The Nitinol-reinforced wall yielded at a displacement five times greater than the steel-reinforced wall, but at a corresponding lateral load that was 4% smaller, indicating a lower initial secant stiffness of the structure. This is due to the lower modulus of elasticity of the Nitinol SMA bars in the boundaries compared to the steel reinforcing bars.

4. The Nitinol-reinforced wall reached an ultimate displacement 72% greater than the steel-reinforced wall, at a load greater by 12%. However, SWN appears to have one-third the ductility of the conventional steel-reinforced wall relative to a lower initial secant stiffness.

7 REFERENCES

Abdulridha, A. 2013. Performance of Superelastic Shape Memory Alloy Reinforced Concrete Elements Subjected to Monotonic and Cyclic Loading. *Ph.D. Thesis*, University of Ottawa, 1-346.

Abdulridha, A., Palermo, D., Foo, S., and Vecchio, F. J. 2013. Behavior and Modelling of Superelastic Shape Memory alloy Reinforced Concrete Beams. *Engineering Structures*, Elsevier, 49(13): 893-904.

Abdulridha, A., and Palermo, D. 2017. Behaviour and modelling of hybrid SMA-steel reinforced concrete slender shear walls. *Engineering Structures*, Elsevier, 147(2017): 77-89.

Alam, M. S., Nehdi, M., and Youssef, M. A. 2007. Applications of Shape Memory Alloys in Earthquake Engineering. *Ninth Canadian Conference on Earthquake Engineering*, Ottawa: 1468-1477.

ATC-24. 1992. Guidelines for Cyclic Seismic Testing of Components of Steel Structures. AISI.

Cladera, A., Weber, B., Leinenbach, C., Czaderski, C., Shahverdi, M., and Motavalli, M. 2014. Iron-based shape memory alloys for civil engineering structures: An overview. *Construction and Building Materials*, Elsevier, 63(2014): 281-293.

Cortés-Puentes, W. L., and Palermo, D. 2017. Seismic Retrofit of Concrete Shear Walls with Tension-Only SMA Braces. *16th World Conference on Earthquake*, WCEE, 1-11.

CSA A23.3-04. 2004. Design of Concrete Structures. Canadian Standards Association. Rexdale, Canada.

FEMA 461. 2007. Interim Testing Protocols for Determining the Seismic Performance Characteristics of Structural and Nonstructural Components. Applied Technology Council.

Menna, C., Aurricchio, F., and Asprone, D. 2015. Applications of Shape Memory Alloys in Structural Engineering. *Shape Memory Alloys Engineering*, Elsevier, 109(2): 369-403.

Ozbulut, O. E., Hurlebaus, S., and DeRoches, R. 2011. Seismic Response Control Using Shape Memory Alloys: A Review. *Journal of Intelligent Material Systems and Structures,* 0(2011): 1-19.

Park, R. 1989. Evaluation of Ductility of Structures and Structural Assemblages From Laboratory Testing. *Bulletin of the New Zealand National Society for Earthquake Engineering*, 22(3): 155-166.

Saiidi, M., and Wang, H. 2006. Exploratory Study of Seismic Response of Concrete Columns with Shape Memory Alloys Reinforcement. *Structural Journal*, ACI, 436-443.

Shahverdi, M., Czaderski, C., Annen, P., and Motavalli, M. 2016. Strengthening of RC beams by iron-based shape memory alloy bars embedded in a shotcrete layer. *Engineering Structures*, Elsevier, 117(2016): 263-273.

Tazarv, M., and Saiidi, S. 2017. Analysis, Design, and Construction of SMA-Reinforced FRP-Confined Concrete Columns. *Fourth Conference on Smart Monitoring, Assessment and Rehabilitation of Civil Structures*, SMAR 2017, Zürich, Switzerland.

Yazgan, U. 2010. The Use of Post-Earthquake Residual Displacement as a Performance Indicator in seismic Assessment. *IBK Bericht*, ETH Zurich, 330(2010): 1-232.

Youssef, M. A., Alam, M. S., and Nehdi, M. 2008. Experimental Investigation on the Seismic Behavior of Beam-Column Joints Reinforced with Superelastic Shape Memory Alloys. *Journal of Earthquake Engineering*, 12(2008): 1205-1222.